SOFTENED SYMBOL GROUNDING FOR NEURO-SYMBOLIC SYSTEMS

Anonymous authors
Paper under double-blind review

ABSTRACT

Neuro-symbolic learning usually consists of two worlds, i.e., neural network learning and symbolic constraint satisfaction, whose effectiveness hinges on symbol grounding, a fundamental problem in AI. This paper presents a novel, softened symbol grounding process, enabling the interactions of the two worlds in a mutually beneficial manner. Technically, we design a neuro-symbolic learning framework that features (1) modeling of deterministic symbol solution states as a Boltzmann distribution, which avoids expensive state searching and facilitates the interaction between network training and symbolic reasoning; (2) an efficient MCMC sampling technique leveraging projection and SMT solvers, which overcomes the connectivity barrier in sampling symbol solution spaces; (3) an annealing mechanism that avoids the trap of sub-optimal symbol groundings. Experiments with three representative neuro-symbolic learning tasks demonstrate that, thanks to its superior symbol grounding capability, our framework successfully solves problems well beyond the frontier of the existing proposals.

1 INTRODUCTION

Neuro-symbolic systems have been proposed to connect neural network learning and symbolic constraint satisfaction (Garcez et al., 2019; Marra et al., 2021; Yu et al., 2021; Hitzler, 2022). In these systems, the neural network component first recognizes the raw input as a symbol, which is further fed into the symbolic component to produce the final output (Yi et al., 2018; Li et al., 2020; Liang et al., 2017). Such a neuro-symbolic paradigm has shown unprecedented capability and achieved impressive results in many tasks including visual question answering (Yi et al., 2018; Vedantam et al., 2019; Amizadeh et al., 2020), vision-language navigation (Anderson et al., 2018; Fried et al., 2018), and math word problem solving (Hong et al., 2021; Qin et al., 2021), to name a few.

An example of a neuro-symbolic system is shown in Figure 1, where the system takes a handwritten arithmetic expression as the input and aims to evaluate the expression. In this task, the neural network component recognizes the symbols (i.e., digits and operators) in the expression, and the symbolic component evaluates the recognized formula by, e.g., the Python function 'eval'. To maximize the generalizability, such problems are usually cast as a weakly-supervised task (Garcez et al., 2022): the final value of the expression, rather than the intermediate label of each digit or operator, is provided as the supervision during training.

Lacking directly supervised labels for the intermediate symbols appeals for an effective and efficient approach to solving the symbol grounding problem, i.e., establishing a feasible and generalizable mapping from the raw input to the latent symbols. Although some existing methods tend to bypass the grounding by parsing the final output to the corresponding symbolic constraint (Manhaeve et al., 2018; Xu et al., 2018; Pryor et al., 2022), they cannot achieve a satisfactory performance without explicit symbol labels. On the other hand, some efforts have been devoted to the grounding problem by incorporating it into network learning (Dai et al., 2019; Li et al., 2020), but they often highly depend on a good initial model and are ineffective when starting from scratch (Huang et al., 2021).

Our key insight is to improve the interactions between the neural perception and symbolic reasoning, so as to boost the efficacy of symbol grounding. To this end, we propose to soften the symbol grounding. That is, instead of searching for a deterministic input-symbol mapping, we optimize their Boltzmann distribution, with an annealing strategy to gradually converge to the deterministic one. From the perspective of game theory, the softening forms a series of mixed strategy games during

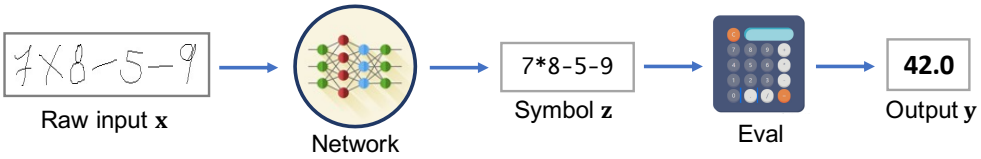

Figure 1: An example neural-symbolic system for handwritten formula evaluation.

the annealing process, which encourages stronger interactions and thus obtains a strict improvement of the utility (Conitzer, 2016).

Furthermore, the softening approach allows us to solve the original bi-level optimization by the (min-oracle) stochastic gradient descent (Jin et al., 2020). To avoid the sparsity problem and obtain the gradient estimate efficiently, we sample the Boltzmann distribution directly from the solution space (i.e., all symbols satisfying the symbolic constraint), rather than the entire symbol space as the existing methods did. However, the poor connectivity between different solutions would significantly increase the mixing time of Markov Chain Monte Carlo (MCMC) sampling. To overcome this deficiency, we leverage the projection technique to accelerate the random walk for sampling (Feng et al., 2021b), aided by satisfiability modulo theory (SMT) solvers (Nieuwenhuis et al., 2006; Moura & Bjørner, 2008). Namely, the projection can significantly improve the connectivity of different solutions, and, by applying the SMT solver as the inverse projection, the random walk can be easily conducted in the projection space, ensuring that the MCMC sampling has a rapid mixing time (Feng et al., 2021a). It is known that MCMC sampling and SMT solvers may introduce bias, but our theoretical result confirms that it can be pleasantly offset by stochastic gradient descent adopted in the algorithm. Experiments on various typical neural-symbolic tasks, including handwritten expression evaluation, visual Sudoku classification, and shortest path search, demonstrate the superior performance of the proposed method over the state-of-the-art methods.

2 Softening Symbol Grounding

Throughout this paper, we refer to $\mathcal{X}$ as the input space of the neuro-symbolic system, and $\mathcal{Z}$ as its *symbol space* or *state space* (e.g., all legal and illegal arithmetic expressions in the HWF task). We consider the neuro-symbolic computing task which first trains a neural network (parameterized by $\boldsymbol{\theta}$), mapping a raw input $\mathbf{x} \in \mathcal{X}$ to some latent state $\mathbf{z} \in \mathcal{Z}$ with a (variational) probability distribution $P_{\boldsymbol{\theta}}(\mathbf{z}|\mathbf{x})$. The state $\mathbf{z}$ is further fed into a predefined symbolic reasoning procedure to produce the final output $\mathbf{y}$. The training data contains only the input $\mathbf{x}$'s and the corresponding $\mathbf{y}$'s, which casts the problem into the so-called weakly-supervised setting. In general, we formulate the pre-defined symbolic reasoning procedure and the output $\mathbf{y}$ as a set of *symbolic constraint* $\mathcal{S}_{\mathbf{y}}$ on the symbol space. For instance, in Figure 1, the constraint specifies that the arithmetic expressions must evaluate to 42. We say a state $\mathbf{z}$ is *feasible* or satisfies the symbolic constraint if $\mathbf{z} \in \mathcal{S}_{\mathbf{y}}$.

The major challenge in this neuro-symbolic learning paradigm lies in the *symbol grounding problem*, i.e., establishing a mapping $h\colon \mathcal{X} \to \mathcal{Z}$ from the raw input to a feasible state that satisfies the symbolic constraint. Specifically, an effective mapping h should enable the model to explain as many observations as possible. As a result, the symbol grounding problem on a given dataset $\{(\mathbf{x}^i, \mathbf{y}^i)\}_{i=1,\ldots,N}$ can be formulated as

$$\min_{h} \left\{ \min_{\boldsymbol{\theta}} \ell(\boldsymbol{\theta}) := -\sum_{i=1}^{N} \log P_{\boldsymbol{\theta}}(\mathbf{z}^i|\mathbf{x}^i) \right\} \quad \text{s.t.} \quad \mathbf{z}^i = h(\mathbf{x}^i) \in \mathcal{S}_{\mathbf{y}^i}, i = 1, \ldots, N. \tag{1}$$

A straightforward solution to the above formulation would first train a network for each feasible mapping, and then select the one that achieves the final output $\mathbf{y}$ with a maximum likelihood. However, this solution is impractical since the number of feasible mappings grows exponentially.

An obvious shortcoming of the above solution is that the neural network learning process makes no use of the knowledge embodied in the symbolic constraint. Vice versa, the searching for the best mapping is not guided by the network. To overcome this shortcoming, one can switch the

minimization order in problem (1), and obtain a new but numerically equivalent problem:

$$\min_{\boldsymbol{\theta}} \left\{ \min_{h} \ell(\boldsymbol{\theta}) := -\sum_{i=1}^{N} \log P_{\boldsymbol{\theta}}(\mathbf{z}^i|\mathbf{x}^i) \quad \text{s.t.} \quad \mathbf{z}^i = h(\mathbf{x}^i) \in \mathcal{S}_{\mathbf{y}^i}, i = 1, \ldots, N \right\}. \tag{2}$$

The optimization problem (2) first determines a "best" mapping based on the initial model, and then updates the model to fit this mapping. The two steps are iterated until no improvement can be made. However, this grounding strategy may easily get trapped into a local optimum. The reason is that, every time a feasible mapping h is achieved, h tends to direct the neural network to (over)fit itself. Because the mappings are deterministic and discrete, there is no smooth route to alternative feasible mappings that would further improve the network. This insufficient information exchange between network training and symbolic reasoning makes the success of symbol grounding highly dependent on the quality of the initial model, which causes the troublesome cold start problem.

In this work, we propose to soften the symbol grounding to facilitate the interaction between neural perception and symbolic reasoning. Elaborately, instead of directly searching for a deterministic mapping h, we first pursue an optimal probability distribution of h, and then gradually "sharpen" the distribution to obtain the final deterministic h. Formally, for each input $\mathbf{x}$, we introduce a Boltzmann distribution $Q_{\boldsymbol{\phi}}$ over $\mathcal{S}_{\mathbf{y}}$, parameterized by $\boldsymbol{\phi}$, to indicate the probability of each feasible state that satisfies the symbolic constraint. Then, the softened symbol grounding problem can be formulated as follows:

$$\begin{aligned} \min_{\boldsymbol{\theta},\boldsymbol{\phi}} \quad & \ell(\boldsymbol{\theta}, \boldsymbol{\phi}) := -\sum_{i=1}^{N} \sum_{\mathbf{z}^i \in \mathcal{S}_{\mathbf{y}}^i} Q_{\boldsymbol{\phi}}^i(\mathbf{z}^i) \log P_{\boldsymbol{\theta}}(\mathbf{z}^i|\mathbf{x}^i) + \gamma Q_{\boldsymbol{\phi}}^i(\mathbf{z}^i) \log Q_{\boldsymbol{\phi}}^i(\mathbf{z}^i) \\ \text{s.t.} \quad & \text{supp}(Q_{\boldsymbol{\phi}}^i) \subseteq \mathcal{S}_{\mathbf{y}^i}, \quad i = 1, \ldots, N, \end{aligned} \tag{P}$$

where $\text{supp}(Q_{\boldsymbol{\phi}})$ denotes the support of $Q_{\boldsymbol{\phi}}$. The entropy term $\sum_{\mathbf{z} \in \mathcal{S}_{\mathbf{y}}} Q_{\boldsymbol{\phi}}(\mathbf{z}) \log Q_{\boldsymbol{\phi}}(\mathbf{z})$ is introduced to control the sharpness of $Q_{\boldsymbol{\phi}}$ (MacKay et al., 2003), and the decreasing of its coefficient γ ensures that the grounding can converge to a deterministic mapping h. Except for the case $\gamma = 1$ which yields the KL divergence between $P_{\boldsymbol{\theta}}$ and $Q_{\boldsymbol{\phi}}$, we also examine two extreme cases: (1) when $\gamma \to +\infty$, $Q_{\boldsymbol{\phi}}$ is forced towards the uniform distribution, and thus the minimization only aims to restrict the support of $P_{\boldsymbol{\theta}}$ to $\mathcal{S}_{\mathbf{y}}$; (2) when $\gamma \to 0$, $Q_{\boldsymbol{\phi}}$ is confined to a one-hot categorical distribution, reducing to directly search for the deterministic mapping h.

Advantages. Game theory provides a perspective to understand why our softened strategy improves over problems (1) and (2) with a better interaction between model training and symbolic reasoning. Either problem (1) or (2) can be viewed as a Stackelberg game with pure strategies, in which the player takes a single action (i.e., selecting a deterministic mapping h). However, in problem (P), the player takes a randomized action with the distribution $Q_{\boldsymbol{\phi}}$. Such a mixed strategy does provide more information of the game, and thus strictly improves the utility (Letchford et al., 2014).[1]

In addition, this softening technique also avoids enumeration and thus improves efficiency. In problem (1), for each input $\mathbf{x}$, the minimization in its corresponding symbol $\mathbf{z}$ needs searching over the whole $\mathcal{S}_{\mathbf{y}}$ (i.e., enumerating all feasible states satisfying the symbolic constraint). This is generally an intractable *#P-complete* problem in theory (Arora & Barak, 2009). Problem (P) circumvents this costly computation by estimating the expectation over $Q_{\boldsymbol{\phi}}$, which can be efficiently computed with a tailored sampling strategy discussed in the next section.

3 Markov chain Monte Carlo Estimate via Projection

To easy presentation, in this section, we consider a single data sample. Specifically, by removing the summation over all samples and dropping the superscripts, problem (P) can be formulated as

$$\min_{\boldsymbol{\theta},\boldsymbol{\phi}} \ \ell(\boldsymbol{\theta}, \boldsymbol{\phi}) := \sum_{\mathbf{z} \in \mathcal{S}_{\mathbf{y}}} Q_{\boldsymbol{\phi}}(\mathbf{z}) \log P_{\boldsymbol{\theta}}(\mathbf{z}|\mathbf{x}) + \gamma Q_{\boldsymbol{\phi}}(\mathbf{z}) \log Q_{\boldsymbol{\phi}}(\mathbf{z}), \quad \text{supp}(Q_{\boldsymbol{\phi}}) \subseteq \mathcal{S}_{\mathbf{y}}. \tag{3}$$

This problem can be solved by alternating between the gradient descent step in $\boldsymbol{\theta}$ and the minimization step in $\boldsymbol{\phi}$. The updates of $\boldsymbol{\theta}$ and $\boldsymbol{\phi}$ at the k-th iteration are

$$\boldsymbol{\theta}_{k+1} = \boldsymbol{\theta}_k - \eta \nabla_{\boldsymbol{\theta}} \ell(\boldsymbol{\theta}_k, \boldsymbol{\phi}_k), \quad \boldsymbol{\phi}_{k+1} = \underset{\boldsymbol{\phi}|\text{supp}(Q_{\boldsymbol{\phi}})}{\arg\min} \ \ell(\boldsymbol{\theta}_{k+1}, \boldsymbol{\phi}). \tag{4}$$

[1] Conitzer (2016) provides a nice illustrative example, which one may consult for more details.

Note that the closed-form solution $Q_{\boldsymbol{\phi}^*}$ exists when $P_{\boldsymbol{\theta}}$ is fixed, ensuring the convergence of gradient descent in $\boldsymbol{\theta}$ (Jin et al., 2020, Theorem 31). For details, the lower-level problem, i.e., $\min_{\boldsymbol{\phi}} \ell(\boldsymbol{\theta}, \boldsymbol{\phi})$, is strictly convex, and thus contains the unique minimum:

$$Q_{\boldsymbol{\phi}^*}(\mathbf{z}) = \begin{cases} P_{\boldsymbol{\theta}}(\mathbf{z}|\mathbf{x})^{\frac{1}{\gamma}} / \sum_{\mathbf{z}' \in \mathcal{S}_{\mathbf{y}}} P_{\boldsymbol{\theta}}(\mathbf{z}'|\mathbf{x})^{\frac{1}{\gamma}}, & \text{if } \mathbf{z} \in \mathcal{S}_{\mathbf{y}}, \\ 0, & \text{otherwise.} \end{cases} \tag{5}$$

Given the closed-form solution $Q_{\boldsymbol{\phi}^*}$, the loss function $\ell(\boldsymbol{\theta}, \boldsymbol{\phi}^*)$ and its gradient $\nabla_{\boldsymbol{\theta}} \ell(\boldsymbol{\theta}, \boldsymbol{\phi}^*)$ can be estimated through Monte Carlo sampling on $Q_{\boldsymbol{\phi}^*}$.

The remaining problem is how to sample $Q_{\boldsymbol{\phi}^*}$, which is challenging due to the unknown structure of $\mathcal{S}_{\mathbf{y}}$. Existing methods usually sample from the entire symbol/state space $\mathcal{Z}$, and then either reject the state $\mathbf{z} \notin \mathcal{S}_{\mathbf{y}}$ (e.g., policy-gradient method (Williams, 1992)), or project the infeasible state $\mathbf{z}$ to $\mathcal{S}_{\mathbf{y}}$ (e.g., back-search method (Li et al., 2020)). Unfortunately, these methods suffer from the *sparsity problem*, i.e., feasible $\mathbf{z}$'s are very sparse in $\mathcal{Z}$, causing the policy-gradient to vanish and the back-search to fail.

To overcome the sparsity problem, we propose to directly sample from the symbolic constraint $\mathcal{S}_{\mathbf{y}}$ (i.e., the solution space). By applying the Metropolis algorithm, the acceptance ratio of jumping from one feasible state $\mathbf{z}$ to another one $\mathbf{z}'$ does not vanish, and can be computed as

$$\tau = \frac{Q_{\boldsymbol{\phi}^*}(\mathbf{z}')}{Q_{\boldsymbol{\phi}^*}(\mathbf{z})} = \left(\frac{P_{\boldsymbol{\theta}}(\mathbf{z}'|\mathbf{x})}{P_{\boldsymbol{\theta}}(\mathbf{z}|\mathbf{x})} \right)^{\frac{1}{\gamma}}. \tag{6}$$

Hence the problem becomes: (1) how to generate an initial state $\mathbf{z}$, and (2) how to jump from $\mathbf{z}$ to $\mathbf{z}'$. For the former, a natural way is to leverage SMT solvers (Moura & Bjørner, 2008).[2] For the latter, the most commonly used strategy is to achieve the new state via random walk (Sherlock et al., 2010). However, there lacks a systematic random walk approach in the solution space, because the solution space is likely unconnected (Wigderson, 2019), creating the so-called *connectivity barrier*.

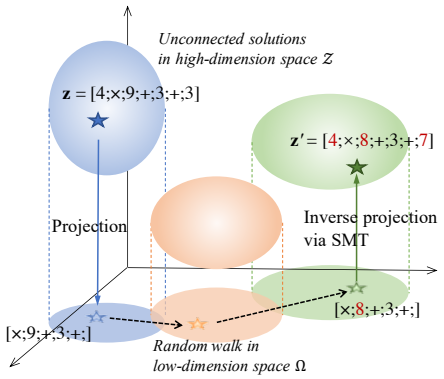

Figure 2: Sampling unconnected solutions via projection. For our running example, we use the projection $\Pi([\mathbf{z}_1; \ldots; \mathbf{z}_7]) = [\mathbf{z}_2; \ldots; \mathbf{z}_6]$, i.e., dropping the first and the last digits. The current state $\mathbf{z} = [4; \times; 9; +; 3; +; 3]$ is projected to $\Pi(\mathbf{z}) = [\times; 9; +; 3; +;]$. We than randomly select an individual component, say, '9', and update it to '8'. Next, a new feasible state (e.g., 4×8+3+7=42) is derived by computing the inverse projection of $\Pi(\mathbf{z}') = [\times; 8; +; 3; +;]$ with an SMT solver.

Inspired by Feng et al. (2021a), we propose to overcome the connectivity barrier by the *projection* technique. Elaborately, we introduce a projection operator $\Pi(\cdot)\colon \mathcal{Z} \to \Omega$ that maps the state space $\mathcal{Z}$ to a lower-dimension space Ω, and then apply the single-site Metropolis algorithm in Ω. The projection essentially compacts the state space, and thus significantly improves the connectivity of the solution space. Figure 2 illustrates the key idea. Consider the running example in Figure 1, where $\mathcal{S}_{\mathbf{y}}$ requires that all expressions are evaluated to 42. The SMT solver, together with the standard single-site Metropolis (a.k.a. Metropolis-in-Gibbs) (Metropolis et al., 1953; Bai, 2009), can easily derive an initial state (e.g., 4×9+3+3) satisfying the symbolic constraint, but cannot further explore other feasible states due to the connectivity barrier (Ermon et al., 2012).[3] In contrast, in the lower-dimension space Ω, it is much easiler to jump to another feasible state.

[2]Current SMT solvers are mainly designed for the satisfaction problem, namely, they are efficient in finding a solution, but underperform in generating all solutions.

[3]To maintain stability, the single-site Metropolis conducts random walk in a component-wise way. That is, in each iteration, it randomly selects and updates an individual component in the current state $\mathbf{z}$ to generate a new state $\mathbf{z}'$. However, it can be observed that the update of any individual component (i.e., '4','×', '9', '+', '3', '+', '3') will result in no feasible new states.

Algorithm 1 Neural Symbolic Learning Procedure

Set an initial value of γ.
Calculate an initial state $\mathbf{z} \in \mathcal{S}_{\mathbf{y}}$ for each input-output pair $(\mathbf{x}, \mathbf{y})$ via the SMT solver.
for $k = 0, 1, \ldots, K$ **do**
  Randomly draw an example $(\mathbf{x}, \mathbf{y})$ from training data $\{(\mathbf{x}_i, \mathbf{y}_i)\}_{i=1}^N$.
  for $t = 0, 1, \ldots, T$ **do**
    Generate new state
    Compute the projection $\boldsymbol{u} = \Pi(\mathbf{z}) \in \Omega$.
    Obtain $\boldsymbol{u}'$ by randomly selecting and updating a component of $\boldsymbol{u}$.
    Calculate the inverse projection $\mathbf{z}' = \Pi^{-1}(\boldsymbol{u}')$ via the SMT solver, as a new state.
    Accept/reject new state
    Calculate the acceptance ratio $\tau = (P_{\boldsymbol{\theta}}(\mathbf{z}'|\mathbf{x})/P_{\boldsymbol{\theta}}(\mathbf{z}|\mathbf{x}))^{1/\gamma}$.
    Generate a uniform random number $\nu \in [0, 1]$.
    Update the state $\mathbf{z}$ to $\mathbf{z}'$ if $\nu \leq \tau$.
  end for
  Train the network
  Estimate the gradient $\hat{\nabla}\ell(\boldsymbol{\theta}) = -\nabla_{\boldsymbol{\theta}} \log P_{\boldsymbol{\theta}}(\mathbf{z}|\mathbf{x})$.
  Update network parameters $\boldsymbol{\theta}$ by the stochastic gradient decent.
  Decrease the coefficient γ.
end for

4 Algorithm and Analysis

The overall algorithm of our neuro-symbolic learning is shown in Alg. 1. In a nutshell, we first conduct a few random walk steps to sample a new state $\mathbf{z}$ on the distribution $Q_{\boldsymbol{\phi}^*}$; we then estimate the gradient based on $\mathbf{z}$, and conduct one stochastic gradient descent step. As shown by Feng et al. (2021a), under some proper assumptions, the Metropolis algorithm enjoys the *rapid mixing* property on the projection space (Levin & Peres, 2017). Therefore, we can efficiently construct the approximate sampling on $Q_{\boldsymbol{\phi}^*}$, without taking too many steps in the Metropolis algorithm. Additionally, both the sampling method and the SMT solver can be paralleled for different examples, hence the batch gradient descent is well supported in our framework.

Convergence. In the ideal case, the gradient estimate $\hat{\nabla}\ell(\boldsymbol{\theta})$ is unbiased, and the gradient descent in $\boldsymbol{\theta}$ (i.e., the network parameters) can converge. However, the bias is introduced due to: 1) the approximate sampling of Metropolis algorithm (Jacob et al., 2017); 2) the inverse projection implemented by the SMT solver (Moura & Bjørner, 2008). For the former, we have to increase the number of inner iterations in our algorithm, or consider adaptive variants of the Metropolis algorithm. For the latter, we can alter the projection operator during the training process, or increase the dimension of projection space. Nevertheless, none of these methods can fully avoid the bias of gradient estimate. To this end, we provide a convergence result for the stochastic gradient descent with limited bias.

Proposition 1. *Assume the loss function $\ell(\boldsymbol{\theta})$ is L-Lipschitz and ℓ-smooth, and let the actual sampling distribution be $\widehat{Q}$. Then, if the total variation distance $d_{tv}(\widehat{Q}, Q^*)$ is bounded by ϵ, it holds after K steps of the stochastic gradient descent with learning rate $\eta = \alpha/(\sqrt{T+1})$:*

$$\frac{1}{K}\sum_{k=1}^{K} \|\nabla \ell(\boldsymbol{\theta}_k)\|^2 \leq \mathcal{O}\left(\frac{\ell\sigma^2 + \Delta_0}{\alpha\sqrt{T+1}}\right) + (n\epsilon L)^2,$$

where $\Delta_0 = \ell(\boldsymbol{\theta}_0) - \min \ell(\boldsymbol{\theta})$, and n is the cardinal number of $\mathrm{supp}(Q^*)$.

Remarks. The proof is in Appendix A.1, which is a direct result of Ajalloeian & Stich (2020, Lemma 3). This proposition states that the stochastic gradient descent with MCMC gradient estimate converges to an approximate stationary point. Moreover, the bias term is gradually wiped out in the training process, since the decreasing of γ shrinks the support of Q^*, making the gradient estimate finally be aligned with the true one.

Generalization of existing methods. Existing neuro-symbolic learning frameworks, viz. semantic loss (Xu et al., 2018), deepproblog (Manhaeve et al., 2018), and neural-grammar-symbolic learning (Li et al., 2020), can be understood as special cases of our framework.

Proposition 2. *All the three frameworks (semantic loss, deepproblog, and neural-grammar-symbolic learning) share the same loss function*

$$\hat{\ell}(\boldsymbol{\theta}) := -\sum_{i=1}^{N} \sum_{\mathbf{z}^i \in \mathcal{S}_{\mathbf{y}}^i} \log P_{\boldsymbol{\theta}}(\mathbf{z}^i|\mathbf{x}^i), \tag{7}$$

and they are equivalent to Problem (P) with a fixed γ ($\gamma = 1$). Here, the equivalence means that the problems have the same optimal solution and gradient descent dynamics.

Remarks. A proof is given in Appendix A.2. Compared with minimizing equation 7, our framework enjoys two advantages: (i) the Boltzmann distribution Q is explicitly expressed, making the sampling tractable and easy-to-implement even when the state space is very large; (ii) the annealing strategy of γ largely alleviates the sensitivity to the initial point, guiding to a better optimal solution (Van Laarhoven & Aarts, 1987).

Annealing strategy. Next, we discuss the decreasing strategy of γ. By setting $\boldsymbol{\phi}_{\mathbf{z}}^* = -\log P_{\boldsymbol{\theta}}(\mathbf{z}|\mathbf{x})$ as the entropy for each state $\mathbf{z}$ (Thomas & Joy, 2006), we can obtain that

$$Q_{\boldsymbol{\phi}^*}(\mathbf{z}) = \frac{\exp(-\boldsymbol{\phi}_{\mathbf{z}}^*/\gamma)}{\sum_{\mathbf{z}' \in \mathcal{S}_{\mathbf{y}}} \exp(-\boldsymbol{\phi}_{\mathbf{z}}^*/\gamma)}. \tag{8}$$

It should be noted that the entropy $\boldsymbol{\phi}_{\mathbf{z}}^*$ is essentially the energy of that state $\mathbf{z}$, and the coefficient γ plays a role of temperature in the Boltzmann distribution (LeCun et al., 2006). From this perspective, it is natural to use some classic annealing (or cooling) schedules to decrease γ (Hajek, 1988; Nourani & Andresen, 1998; Henderson et al., 2003). In this work, we consider the following three schedules: (1) *logarithmic* cooling schedule, i.e., $\gamma_t = \gamma_0/\log(1+t)$; (2) *exponential* cooling schedule, i.e., $\gamma_t = \gamma_0 \alpha^t$; (3) *linear* cooling schedule, i.e., $\gamma_t = \gamma_0 - \alpha t$.

Furthermore, after the annealing stage, i.e., when the temperature is decreased to a small value, we will directly set $\gamma = 0$, and train the network by a few more epochs. It should be noted that, in this zero-degree stage, the problem is essentially reduced to a semi-supervised setting (Lee et al., 2013), in which pseudo labels are determined by the one-hot categorical distribution $Q_{\boldsymbol{\phi}^*}$. Some semi-supervised techniques could be applicable to this case, but are not sufficiently efficient due to the massive state space. Therefore, we use the simplest strategy, i.e., only train by those examples with predicted symbols satisfying the symbolic constraint.

5 Experiments and Results

We carry out experiments on three tasks, viz. handwritten formula calculation (HWF), visual Sudoku classification (Sudoku), and single-destination shortest path prediction in weighted graphs (SDSP). For the proposed approach, we split it into two stages, i.e., I: Annealing (γ-decreasing) stage, and II: Zero-degree ($\gamma = 0$) stage, and separately evaluate Stage-I and Stage-I+II. For the first state, we employ three different cooling schedules (Log, Exp, and Linear) as discussed in Section 4. The projection operator is specific to each task, and the corresponding inverse projection operator is implemented by the Z3 SMT solver (Moura & Bjørner, 2008). Through parallel computation (Joblib Development Team, 2020), Z3 solves the inverse projection (on average) in 2.8ms$\sim$6.4ms per example, which is generally acceptable for batch gradient descent.

We compare our approach with the existing state-of-the-art methods, which can be divided into two categories, viz., policy-gradient-based approaches, and symbolic-parser-based approaches. The former includes RL (i.e., learning with REINFORCE) and MAPO (Liang et al., 2018) (i.e., learning by Memory Augmented Policy Optimization (MAPO)). For the latter, most existing methods (e.g., semantic loss (Xu et al., 2018) and deepproblog (Manhaeve et al., 2018)) are intractable in the studied tasks (Huang et al., 2021). Hence, based on Proposition 2 and borrowing our projection-based MCMC technique, we implement a stochastic version for them (referred to as SSL henceforth) for comparison. More implementation details can be found in Appendix B. The code, together with the experimental data, is available at `https://figshare.com/s/10c155babbb52192becf`.

Method		Symbol	Calculation
Baseline	RL	6.5	0.0
	MAPO	8.7	0.0
	NGS	8.1	0.0
	SSL	70.5	8.4
	NA	55.1	2.83
Ours (Stage I)	Log	81.4	23.2
	Exp	82.6	25.7
	Linear	79.9	19.9
Ours (Stage I+II)	Log	91.0	52.2
	Exp	**98.6**	**90.7**
	Linear	97.6	85.0

Table 1: Accuracy (%) of the HWF task. Our methods (i.e., Stage I+II) perform much better than comparison methods.

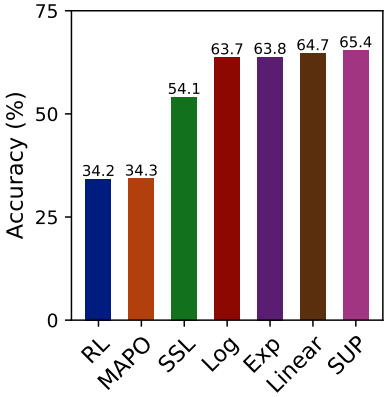

Figure 3: Accuracy (%) of the SDSP task. Our methods are better than competitors and close to the direct supervision case.

5.1 Handwritten Formula Evaluation

We first evaluate our approach on the handwritten formula dataset provided by Li et al. (2020). Since the original dataset consists of formulas with lengths varying from 1 to 7, which may lead to the label leakage problem, we only take the 6K/1.2K formulas with length 7 as the training/test set. In this neuro-symbolic system, the neural network is required to recognize symbols including digits 1-9 and basic operators ($+, -, \times, \div$). The symbolic module evaluates the expression via the Python program 'eval'. In this task, we also compare with the neural-grammar-symbolic (NGS) method (Li et al., 2020), and a special case of our approach with no-annealing strategy (NA). For SSL, NA, and our approach, we define the projection operator as $\Pi(\mathbf{z}_1; \ldots; \mathbf{z}_7) = [\mathbf{z}_1; \mathbf{z}_2; \mathbf{z}_4; \mathbf{z}_6; \mathbf{z}_7]$, i.e., drop the third and fifth symbols in the formula.[4]

We report the symbol accuracy (i.e., the percentage of symbols that are correctly predicted) and the calculation accuracy (i.e., the percentage of final results that are correctly calculated) in Table 1. Observe that our approaches (Log, Exp, and Linear) significantly outperform the competitors. Additionally, when Stage-II is included, both symbol accuracy and (especially) calculation accuracy can be further improved. Note that the final calculation accuracy of our methods are dramatically better than all the competitors, even when the symbol accuracy is relatively closer. This is due to the fact that our softened symbol grounding allows the two modules to continuously adjust themselves, so as to achieve a much better overall result. Overall, our two stage algorithm with the Exp annealing strategy achieves the best performance on both symbol accuracy and calculation accuracy. The Log annealing strategy in Stage II cannot obtain a comparable result with the other two strategies, because its temperature is not reduced to a sufficiently low value. Additional learning curve results and analysis can be found in Appendix B.3.

5.2 Visual Sudoku Classification

We next evaluate our approach on a visual Sudoku classification task (Wang et al., 2019), where the neural network recognizes the digits (i.e., MNIST images) in the Sudoku board, and the symbolic module determines whether a solution is valid for the puzzle. To evaluate the sample efficiency of our approach, we vary the size of training set by 50, 100, 300, and 500, and the size of test set is fixed to 1,000. Note that the solution space in this task is intrinsically connected. For example, one can easily obtain a new solution by permuting any two digits. Therefore, we additionally include this strategy without the projection (denoted by MCMC) as a baseline.

[4]We observe that the solution space is well-connected through different projections. For example, for the used projection with initial $\gamma_0 = 1.0$, around 46% solutions successfully jump to other solutions in an epoch.

Table 2: Accuracy (%) of the Sudoku task. Our methods significantly outperform the competitors.

Method		Number of training puzzles			
		50	100	300	500
Baseline	RL	0.0	0.0	0.0	0.0
	MAPO	0.0	0.0	0.0	0.0
	SSL	5.8	1.6	0.0	0.2
	MCMC	24.3	49.5	63.4	69.8
Ours (Stage I)	Log	30.7	74.7	85.9	86.0
	Exp	33.6	76.5	77.4	89.3
	Linear	46.3	66.8	79.4	84.1
Ours (Stage I+II)	Log	64.8 (35)	82.2 (85)	**93.5 (279)**	92.9 (474)
	Exp	66.3 (39)	**85.5 (94)**	92.3 (274)	**95.4 (480)**
	Linear	**66.9 (41)**	81.5 (85)	90.8 (273)	94.0 (478)

For a given 4-by-4 Sudoku puzzle, we divide it into four disjoint 2-by-2 subboards, and the projection drops the anti-diagonal two. In the projection space, we randomly switch two digits in different rows or columns, and the following example illustrates the whole projection process.

$$\begin{array}{|c|c|c|c|}\hline 2&4&3&1\\\hline 3&1&4&2\\\hline 4&2&1&3\\\hline 1&3&2&4\\\hline\end{array}\xrightarrow{\text{Projection}}\begin{array}{|c|c|c|c|}\hline 2&4&&\\\hline 3&1&&\\\hline &&1&3\\\hline &&2&4\\\hline\end{array}\xrightarrow{\text{Random walk}}\begin{array}{|c|c|c|c|}\hline 2&4&&\\\hline 3&1&&\\\hline &&3&1\\\hline &&2&4\\\hline\end{array}\xrightarrow{\text{Inverse projection}}\begin{array}{|c|c|c|c|}\hline 2&4&1&3\\\hline 3&1&4&2\\\hline 4&2&3&1\\\hline 1&3&2&4\\\hline\end{array}$$

Table 2 shows the accuracy result, i.e., the percentage of correctly predicted boards. It can be seen that RL, MAPO, and SSL fail to obtain a sensible result across all cases. Although the crude MCMC method can achieve a good result, it is still significantly outperformed by our approaches. The reason is that the Markov chain obtained in the original space has slow mixing time, making the MCMC algorithm prone to getting stuck at local minima. To investigate the grounding effect and the sample efficiency, we also report the number of training examples that are correctly grounded (i.e., satisfying the symbolic constraints) in the brackets of Table 2. The result shows the high sample efficiency of our approach. Particularly, with the number of training puzzles increased, the rate of correctly grounded examples has exceeded 90%.

5.3 Shortest Path Search

We finally conduct a single-destination shortest path search task. In this neuro-symbolic system, the symbolic reasoning part implements an A^* search algorithm (Russell, 2010), which maintains a priority queue of the estimated distance $d(n) = g(n) + f_{\boldsymbol{\theta}}(n)$, where n is the next node on the path, $g(n)$ is the known distance from the start node to n, and $f_{\boldsymbol{\theta}}(n)$ is the shortest distance from n to the destination heuristically predicted by a neural network. For simplicity, we set the queue length to 1, i.e., only visit the node with the shortest estimated distance. We randomly generate 3K/1K graphs as training/test set through NetworkX (Hagberg et al., 2008). In each graph, the number of vertices is fixed to 30, and the weights of edges are uniformly sampled among $\{1, 2, \ldots, 9\}$.

For this regression task, we define the symbol $\mathbf{z}$ as a a multivariate Gaussian with diagonal covariance, i.e., $\mathbf{z} \sim \mathcal{N}(f_{\boldsymbol{\theta}}(\mathbf{x}), \sigma^2\mathbf{I})$, where $f_{\boldsymbol{\theta}}(\mathbf{x})$ indicates the predicted distances from all nodes to the given destination. The dimension of $\mathbf{z}$ is 30, and the projection is defined by dropping $[\mathbf{z}_5, \mathbf{z}_{10}, \mathbf{z}_{15}, \mathbf{z}_{20}, \mathbf{z}_{25}]$. The random walk in each step selects a component of $\mathbf{z}$ and adds a uniform noise from $[-5, 5]$ on it.

Figure 3 shows the accuracy results, i.e., the percentage of shortest paths that are correctly obtained. To better understand the effectiveness, we additionally train a reference model (denoted as SUP) with directly supervised labels (i.e., the actual distance from each node to the destination). It can be observed that, our approaches not only outperform the existing competitors, but also achieve a comparable result with the directly supervised model SUP.

6 RELATED WORK

Neuro-symbolic learning. To build a robust computational model integrating concept acquisition and manipulation (Valiant, 2003), neuro-symbolic computing provides an attractive way to reconcile neural learning with logical reasoning. Numerous studies have focused on symbol grounding to enable conceptualization for neural networks. An in-depth introduction can be found in recent surveys (Marra et al., 2021; Garcez et al., 2022). According to the way the symbolic reasoning component is handled, we categorize the existing work as follows.

Learning with logical constraints. Methods in the first category parse the symbolic reasoning into an explicit logical constraint, and then translate the logical constraint into a differentiable loss function which is incorporated as constraints or regularizations in network training. Although several methods, e.g., Hu et al. (2016); Xu et al. (2018); Nandwani et al. (2019); Fischer et al. (2019); Hoernle et al. (2022), are proposed to deal with many different forms of logical constraints, most of them tend to avoid the symbol grounding. In other words, they often only confine the network's behavior, but not guide the conceptualization for the network.

Learning from symbolic reasoning. Another way is to regard the network's output as a predicate, and then maximize the likelihood of a correct symbolic reasoning (a.k.a. learning from entailment (Raedt et al., 2016, Sec. 7)). In some of these methods Manhaeve et al. (2018); Yang et al. (2020); Pryor et al. (2022); Winters et al. (2022), the symbol grounding is often conducted in an implicit manner (as shown by Proposition 2), which limits the efficacy of network learning. Some other methods Li et al. (2020); Dai et al. (2019) achieve an explicit symbol grounding in an abductive way, but still highly depend on a good initial model. Our proposed method falls into this category, but it not only explicitly models the symbol grounding, but also alleviates the sensitivity of the initial model by enabling the interaction between neural learning and symbolic reasoning.

Differentiable logical reasoning. This line of work considers emulating the symbolic reasoning through a differentiable component, and embedding it into complex network architectures. To achieve this goal, a series of techniques Trask et al. (2018); Grover et al. (2019); Wang et al. (2019); Chen et al. (2021) are proposed to approximate different modules in logical reasoning. Despite the success, these methods are still succumb to the symbol grounding problem, and cannot achieve a satisfactory performance without explicit supervision (Topan et al., 2021).

Constrained counting and sampling. Quite a few neuro-symbolic learning methods (Manhaeve et al., 2018; Xu et al., 2018) rely on knowledge compilation (Darwiche & Marquis, 2002), which implements the exact constrained counting based on Binary Decision Diagram (BDD) (Akers, 1978) or Sentential Decision Diagram (SDD) (Darwiche, 2011). Some approximate versions (De Raedt et al., 2007; Manhaeve et al., 2021) are proposed to overcome the computational hardness (Valiant, 1979; Jerrum et al., 1986), but are still inefficient and poorly scalable to large-size problems.

Aided by the progress of SAT/SMT solving (Malik & Zhang, 2009; Vardi, 2014), randomized approximate constrained counting/sampling approaches have been proposed, which are based on hashing (e.g., (Chakraborty et al., 2013; Meel et al., 2016)) or MCMC (e.g. (Wei et al., 2004; Gomes et al., 2006; Ermon et al., 2012)). In particular, previous MCMC-based methods suffer from connectivity barriers. Our approach is based on MCMC, but leverages projection to overcome the connectivity barrier. Moreover, our theoretical result shows that the stochastic gradient descent can offset the possible bias of the gradient estimate introduced by MCMC and SMT solvers.

7 CONCLUSION

In this paper, we present a new neuro-symbolic learning framework for better integrating neural network learning and symbolic reasoning. To focus on the crucial problem of symbol grounding, we limit this work to the scenarios where the symbolic reasoning logic is given as a priori knowledge. The next step is to incorporate the learning of the knowledge into our framework by, e.g., inductive logic programming. Moreover, even though SMT solvers make the projection feasible in a broad range of settings, they might become a bottleneck when instantiating our framework for more complex systems. It would be interesting to consider a substitute of the SMT solver in the neuro-symbolic framework.

REFERENCES

Ahmad Ajalloeian and Sebastian U Stich. On the convergence of sgd with biased gradients. *arXiv preprint arXiv:2008.00051*, 2020.

Sheldon B. Akers. Binary decision diagrams. *IEEE Transactions on computers*, 27(06):509–516, 1978.

Saeed Amizadeh, Hamid Palangi, Alex Polozov, Yichen Huang, and Kazuhito Koishida. Neuro-symbolic visual reasoning: Disentangling. In *International Conference on Machine Learning*, pp. 279–290. PMLR, 2020.

Peter Anderson, Qi Wu, Damien Teney, Jake Bruce, Mark Johnson, Niko Sünderhauf, Ian Reid, Stephen Gould, and Anton Van Den Hengel. Vision-and-language navigation: Interpreting visually-grounded navigation instructions in real environments. In *Proceedings of the IEEE conference on computer vision and pattern recognition*, pp. 3674–3683, 2018.

Sanjeev Arora and Boaz Barak. *Computational complexity: a modern approach*. Cambridge University Press, 2009.

Yan Bai. An adaptive directional metropolis-within-gibbs algorithm. *Preprint*, 2009.

Supratik Chakraborty, Kuldeep S Meel, and Moshe Y Vardi. A scalable approximate model counter. In *International Conference on Principles and Practice of Constraint Programming*, pp. 200–216. Springer, 2013.

Bingqing Chen, Priya L Donti, Kyri Baker, J Zico Kolter, and Mario Bergés. Enforcing policy feasibility constraints through differentiable projection for energy optimization. In *Proceedings of the Twelfth ACM International Conference on Future Energy Systems*, pp. 199–210, 2021.

Vincent Conitzer. On stackelberg mixed strategies. *Synthese*, 193(3):689–703, 2016.

Wang-Zhou Dai, Qiuling Xu, Yang Yu, and Zhi-Hua Zhou. Bridging machine learning and logical reasoning by abductive learning. *Advances in Neural Information Processing Systems*, 32, 2019.

Adnan Darwiche. Sdd: A new canonical representation of propositional knowledge bases. In *Twenty-Second International Joint Conference on Artificial Intelligence*, 2011.

Adnan Darwiche and Pierre Marquis. A knowledge compilation map. *Journal of Artificial Intelligence Research*, 17:229–264, 2002.

Luc De Raedt, Angelika Kimmig, and Hannu Toivonen. Problog: A probabilistic prolog and its application in link discovery. In *IJCAI*, volume 7, pp. 2462–2467. Hyderabad, 2007.

Stefano Ermon, Carla Gomes, and Bart Selman. Uniform solution sampling using a constraint solver as an oracle. In *Proceedings of the Twenty-Eighth Conference on Uncertainty in Artificial Intelligence*, pp. 255–264, 2012.

Weiming Feng, Heng Guo, Yitong Yin, and Chihao Zhang. Fast sampling and counting k-sat solutions in the local lemma regime. *Journal of the ACM (JACM)*, 68(6):1–42, 2021a.

Weiming Feng, Kun He, and Yitong Yin. Sampling constraint satisfaction solutions in the local lemma regime. In *Proceedings of the 53rd Annual ACM SIGACT Symposium on Theory of Computing*, pp. 1565–1578, 2021b.

Marc Fischer, Mislav Balunovic, Dana Drachsler-Cohen, Timon Gehr, Ce Zhang, and Martin Vechev. Dl2: Training and querying neural networks with logic. In *International Conference on Machine Learning*, pp. 1931–1941. PMLR, 2019.

Daniel Fried, Ronghang Hu, Volkan Cirik, Anna Rohrbach, Jacob Andreas, Louis-Philippe Morency, Taylor Berg-Kirkpatrick, Kate Saenko, Dan Klein, and Trevor Darrell. Speaker-follower models for vision-and-language navigation. *Advances in Neural Information Processing Systems*, 31, 2018.

Artur d'Avila Garcez, Marco Gori, Luis C Lamb, Luciano Serafini, Michael Spranger, and Son N Tran. Neural-symbolic computing: An effective methodology for principled integration of machine learning and reasoning. *Journal of Applied Logics*, 6(4):611–632, 2019.

Artur d'Avila Garcez, Sebastian Bader, Howard Bowman, Luis C Lamb, Leo de Penning, BV Illuminoo, Hoifung Poon, and COPPE Gerson Zaverucha. Neural-symbolic learning and reasoning: A survey and interpretation. *Neuro-Symbolic Artificial Intelligence: The State of the Art*, 342:1, 2022.

Carla P Gomes, Ashish Sabharwal, and Bart Selman. Near-uniform sampling of combinatorial spaces using xor constraints. *Advances In Neural Information Processing Systems*, 19, 2006.

Aditya Grover, Eric Wang, Aaron Zweig, and Stefano Ermon. Stochastic optimization of sorting networks via continuous relaxations. In *International Conference on Learning Representations*, 2019.

Aric Hagberg, Pieter Swart, and Daniel S Chult. Exploring network structure, dynamics, and function using networkx. Technical report, Los Alamos National Lab.(LANL), Los Alamos, NM (United States), 2008.

Bruce Hajek. Cooling schedules for optimal annealing. *Mathematics of operations research*, 13(2): 311–329, 1988.

Darrall Henderson, Sheldon H Jacobson, and Alan W Johnson. The theory and practice of simulated annealing. In *Handbook of metaheuristics*, pp. 287–319. Springer, 2003.

Pascal Hitzler. Neuro-symbolic artificial intelligence: The state of the art. 2022.

Nick Hoernle, Rafael Michael Karampatsis, Vaishak Belle, and Kobi Gal. Multiplexnet: Towards fully satisfied logical constraints in neural networks. In *Proceedings of the AAAI Conference on Artificial Intelligence*, volume 36, pp. 5700–5709, 2022.

Yining Hong, Qing Li, Daniel Ciao, Siyuan Huang, and Song-Chun Zhu. Learning by fixing: Solving math word problems with weak supervision. In *Proceedings of the AAAI Conference on Artificial Intelligence*, volume 35, pp. 4959–4967, 2021.

Zhiting Hu, Xuezhe Ma, Zhengzhong Liu, Eduard Hovy, and Eric Xing. Harnessing deep neural networks with logic rules. In *Proceedings of the 54th Annual Meeting of the Association for Computational Linguistics (Volume 1: Long Papers)*, pp. 2410–2420, 2016.

Yu-Xuan Huang, Wang-Zhou Dai, Le-Wen Cai, Stephen H Muggleton, and Yuan Jiang. Fast abductive learning by similarity-based consistency optimization. *Advances in Neural Information Processing Systems*, 34:26574–26584, 2021.

Pierre E Jacob, John O'Leary, and Yves F Atchadé. Unbiased markov chain monte carlo with couplings. *arXiv preprint arXiv:1708.03625*, 2017.

Mark R Jerrum, Leslie G Valiant, and Vijay V Vazirani. Random generation of combinatorial structures from a uniform distribution. *Theoretical computer science*, 43:169–188, 1986.

Chi Jin, Praneeth Netrapalli, and Michael Jordan. What is local optimality in nonconvex-nonconcave minimax optimization? In *International conference on machine learning*, pp. 4880–4889. PMLR, 2020.

Joblib Development Team. Joblib: running python functions as pipeline jobs, 2020. URL `https://joblib.readthedocs.io/`.

Yann LeCun, Sumit Chopra, Raia Hadsell, M Ranzato, and F Huang. A tutorial on energy-based learning. *Predicting structured data*, 1(0), 2006.

Dong-Hyun Lee et al. Pseudo-label: The simple and efficient semi-supervised learning method for deep neural networks. In *Workshop on challenges in representation learning, ICML*, volume 3, pp. 896, 2013.

Joshua Letchford, Dmytro Korzhyk, and Vincent Conitzer. On the value of commitment. *Autonomous Agents and Multi-Agent Systems*, 28(6):986–1016, 2014.

David A Levin and Yuval Peres. *Markov chains and mixing times*, volume 107. American Mathematical Soc., 2017.

Qing Li, Siyuan Huang, Yining Hong, Yixin Chen, Ying Nian Wu, and Song-Chun Zhu. Closed loop neural-symbolic learning via integrating neural perception, grammar parsing, and symbolic reasoning. In *International Conference on Machine Learning*, pp. 5884–5894. PMLR, 2020.

Chen Liang, Jonathan Berant, Quoc Le, Kenneth D. Forbus, and Ni Lao. Neural symbolic machines: Learning semantic parsers on Freebase with weak supervision. In *Proceedings of the 55th Annual Meeting of the Association for Computational Linguistics (Volume 1: Long Papers)*, pp. 23–33, Vancouver, Canada, July 2017. Association for Computational Linguistics. doi: 10.18653/v1/P17-1003. URL https://aclanthology.org/P17-1003.

Chen Liang, Mohammad Norouzi, Jonathan Berant, Quoc V Le, and Ni Lao. Memory augmented policy optimization for program synthesis and semantic parsing. *Advances in Neural Information Processing Systems*, 31, 2018.

David JC MacKay, David JC Mac Kay, et al. *Information theory, inference and learning algorithms*. Cambridge university press, 2003.

Sharad Malik and Lintao Zhang. Boolean satisfiability from theoretical hardness to practical success. *Commun. ACM*, 52(8):76–82, aug 2009. ISSN 0001-0782. doi: 10.1145/1536616.1536637. URL https://doi.org/10.1145/1536616.1536637.

Robin Manhaeve, Sebastijan Dumancic, Angelika Kimmig, Thomas Demeester, and Luc De Raedt. Deepproblog: Neural probabilistic logic programming. *Advances in Neural Information Processing Systems*, 31, 2018.

Robin Manhaeve, Giuseppe Marra, and Luc De Raedt. Approximate inference for neural probabilistic logic programming. In *KR*, pp. 475–486, 2021.

Giuseppe Marra, Sebastijan Dumančić, Robin Manhaeve, and Luc De Raedt. From statistical relational to neural symbolic artificial intelligence: a survey. *arXiv preprint arXiv:2108.11451*, 2021.

Kuldeep S Meel, Moshe Y Vardi, Supratik Chakraborty, Daniel J Fremont, Sanjit A Seshia, Dror Fried, Alexander Ivrii, and Sharad Malik. Constrained sampling and counting: Universal hashing meets sat solving. In *Workshops at the thirtieth AAAI conference on artificial intelligence*, 2016.

Nicholas Metropolis, Arianna W Rosenbluth, Marshall N Rosenbluth, Augusta H Teller, and Edward Teller. Equation of state calculations by fast computing machines. *The journal of chemical physics*, 21(6):1087–1092, 1953.

Leonardo de Moura and Nikolaj Bjørner. Z3: An efficient smt solver. In *International conference on Tools and Algorithms for the Construction and Analysis of Systems*, pp. 337–340. Springer, 2008.

Yatin Nandwani, Abhishek Pathak, and Parag Singla. A primal dual formulation for deep learning with constraints. *Advances in Neural Information Processing Systems*, 32, 2019.

Robert Nieuwenhuis, Albert Oliveras, and Cesare Tinelli. Solving sat and sat modulo theories: From an abstract davis–putnam–logemann–loveland procedure to dpll (t). *Journal of the ACM (JACM)*, 53(6):937–977, 2006.

Yaghout Nourani and Bjarne Andresen. A comparison of simulated annealing cooling strategies. *Journal of Physics A: Mathematical and General*, 31(41):8373, 1998.

Connor Pryor, Charles Dickens, Eriq Augustine, Alon Albalak, William Wang, and Lise Getoor. Neupsl: Neural probabilistic soft logic. *arXiv preprint arXiv:2205.14268*, 2022.

Jinghui Qin, Xiaodan Liang, Yining Hong, Jianheng Tang, and Liang Lin. Neural-symbolic solver for math word problems with auxiliary tasks. In *Proceedings of the 59th Annual Meeting of the Association for Computational Linguistics and the 11th International Joint Conference on Natural Language Processing (Volume 1: Long Papers)*, pp. 5870–5881, Online, August 2021. Association for Computational Linguistics. doi: 10.18653/v1/2021.acl-long.456. URL https://aclanthology.org/2021.acl-long.456.

Luc De Raedt, Kristian Kersting, Sriraam Natarajan, and David Poole. Statistical relational artificial intelligence: Logic, probability, and computation. *Synthesis lectures on artificial intelligence and machine learning*, 10(2):1–189, 2016.

Stuart J Russell. *Artificial intelligence a modern approach*. Pearson Education, Inc., 2010.

Chris Sherlock, Paul Fearnhead, and Gareth O Roberts. The random walk metropolis: linking theory and practice through a case study. *Statistical Science*, 25(2):172–190, 2010.

MTCAJ Thomas and A Thomas Joy. *Elements of information theory*. Wiley-Interscience, 2006.

Sever Topan, David Rolnick, and Xujie Si. Techniques for symbol grounding with satnet. *Advances in Neural Information Processing Systems*, 34:20733–20744, 2021.

Andrew Trask, Felix Hill, Scott E Reed, Jack Rae, Chris Dyer, and Phil Blunsom. Neural arithmetic logic units. *Advances in neural information processing systems*, 31, 2018.

Leslie G Valiant. The complexity of enumeration and reliability problems. *SIAM Journal on Computing*, 8(3):410–421, 1979.

Leslie G Valiant. Three problems in computer science. *Journal of the ACM (JACM)*, 50(1):96–99, 2003.

Peter JM Van Laarhoven and Emile HL Aarts. Simulated annealing. In *Simulated annealing: Theory and applications*, pp. 7–15. Springer, 1987.

Moshe Y Vardi. Boolean satisfiability: theory and engineering. *Communications of the ACM*, 57 (3):5–5, 2014.

Ramakrishna Vedantam, Karan Desai, Stefan Lee, Marcus Rohrbach, Dhruv Batra, and Devi Parikh. Probabilistic neural symbolic models for interpretable visual question answering. In Kamalika Chaudhuri and Ruslan Salakhutdinov (eds.), *Proceedings of the 36th International Conference on Machine Learning*, volume 97 of *Proceedings of Machine Learning Research*, pp. 6428–6437. PMLR, 09–15 Jun 2019. URL https://proceedings.mlr.press/v97/vedantam19a.html.

Po-Wei Wang, Priya Donti, Bryan Wilder, and Zico Kolter. Satnet: Bridging deep learning and logical reasoning using a differentiable satisfiability solver. In *International Conference on Machine Learning*, pp. 6545–6554. PMLR, 2019.

Wei Wei, Jordan Erenrich, and Bart Selman. Towards efficient sampling: Exploiting random walk strategies. In *AAAI*, volume 4, pp. 670–676, 2004.

Avi Wigderson. Mathematics and computation. In *Mathematics and Computation*. Princeton University Press, 2019.

Ronald J Williams. Simple statistical gradient-following algorithms for connectionist reinforcement learning. *Machine learning*, 8(3):229–256, 1992.

Thomas Winters, Giuseppe Marra, Robin Manhaeve, and Luc De Raedt. Deepstochlog: Neural stochastic logic programming. In *Proceedings of the AAAI Conference on Artificial Intelligence*, volume 36, pp. 10090–10100, 2022.

Jingyi Xu, Zilu Zhang, Tal Friedman, Yitao Liang, and Guy Broeck. A semantic loss function for deep learning with symbolic knowledge. In *International conference on machine learning*, pp. 5502–5511. PMLR, 2018.

Zhun Yang, Adam Ishay, and Joohyung Lee. Neurasp: Embracing neural networks into answer set programming. In *29th International Joint Conference on Artificial Intelligence (IJCAI 2020)*, 2020.

Kexin Yi, Jiajun Wu, Chuang Gan, Antonio Torralba, Pushmeet Kohli, and Josh Tenenbaum. Neural-symbolic vqa: Disentangling reasoning from vision and language understanding. *Advances in neural information processing systems*, 31, 2018.

Dongran Yu, Bo Yang, Dayou Liu, and Hui Wang. A survey on neural-symbolic systems. *arXiv preprint arXiv:2111.08164*, 2021.

Note: for the purposes of open access, the author has applied a CC BY public copyright licence to any author accepted manuscript version arising from this submission.

A PROOFS

A.1 PROOF OF PROPOSITION 1

Proof. We define $\ell(\boldsymbol{\theta}) = \mathbb{E}_{\boldsymbol{z}\sim Q^*} \log P_{\boldsymbol{\theta}}(\mathbf{z}|\mathbf{x})$ as the objective function, and consider the bias of gradient on different distributions $\widehat{Q}$ and Q^*, which is denoted by $m(\boldsymbol{\theta})$.

$$m(\boldsymbol{\theta}) = \mathbb{E}_{\boldsymbol{z}\sim\widehat{Q}} \nabla \log P_{\boldsymbol{\theta}}(\mathbf{z}|\mathbf{x}) - \mathbb{E}_{\boldsymbol{z}\sim Q^*} \nabla \log P_{\boldsymbol{\theta}}(\mathbf{z}|\mathbf{x}) = \sum_{\mathbf{z}\in\mathcal{S}_{\mathbf{y}}} \left(\widehat{Q}(\mathbf{z}) - Q^*(\mathbf{z})\right) \nabla \log P_{\boldsymbol{\theta}}(\mathbf{z}|\mathbf{x}).$$

Note that our sampling strategy ensures that only feasible states will be generated, and thus we have

$$\mathrm{supp}(\widehat{Q}) \subseteq \mathrm{supp}(Q^*) \subseteq \mathcal{S}_{\mathbf{y}}.$$

Hence, through the Cauchy-Schwarz inequality, we can obtain that

$$\begin{aligned}
\|m(\boldsymbol{\theta})\|^2 &= \| \sum_{\mathbf{z}\in\mathcal{S}_{\mathbf{y}}} (\widehat{Q}(\mathbf{z}) - Q^*(\mathbf{z})) \nabla \log P_{\boldsymbol{\theta}}(\mathbf{z}|\mathbf{x}) \|^2 \\
&\leq \sum_{\mathbf{z}\in\mathcal{S}_{Q^*}} (\widehat{Q}(\mathbf{z}) - Q^*(\mathbf{z}))^2 \cdot \sum_{\mathbf{z}\in\mathcal{S}_{Q^*}} \|\nabla \log P_{\boldsymbol{\theta}}(\mathbf{z}|\mathbf{x})\|^2 \leq (n\epsilon L)^2,
\end{aligned}$$

where $\mathcal{S}_{Q^*}$ represents the support of Q^* and n denotes its cardinal number. Now, by applying Lemma 3 in Ajalloeian & Stich (2020), we can obtain that

$$\frac{1}{K}\sum_{k=1}^{K} \|\nabla \ell(\boldsymbol{\theta}_k)\|^2 \leq \mathcal{O}\left(\frac{\ell\sigma^2 + \Delta_0}{\alpha\sqrt{T+1}}\right) + (n\epsilon L)^2,$$

where σ^2 is the bounded variance in gradient estimate. □

A.2 PROOF OF PROPOSITION 2

Proof. It can be observed that the loss function $\hat{\ell}(\boldsymbol{\theta}) := -\log \sum_{\mathbf{z}\in\mathcal{S}_{\mathbf{y}}} P_{\boldsymbol{\theta}}(\mathbf{z}|\mathbf{x})$ is essentially the semantic loss (Xu et al., 2018, Def. 1), as well as the loss used in Deepproblog (Raedt et al., 2016, Sec. 7) and NGS (Li et al., 2020, Eq. 7).

Now, we consider the gradient $\nabla\hat{\ell}(\boldsymbol{\theta})$, which can be computed as

$$\begin{aligned}
\nabla\hat{\ell}(\boldsymbol{\theta}) &= -\sum_{\mathbf{z}\in\mathcal{S}(\mathbf{y})} \frac{1}{\sum_{\mathbf{z}'\in\mathcal{S}(\mathbf{y})} P_{\boldsymbol{\theta}}(\mathbf{z}'|\mathbf{x})} \nabla P_{\boldsymbol{\theta}}(\mathbf{z}|\mathbf{x}), \\
&= -\sum_{\mathbf{z}\in\mathcal{S}(\mathbf{y})} \frac{P_{\boldsymbol{\theta}}(\mathbf{z}|\mathbf{x})}{\sum_{\mathbf{z}'\in\mathcal{S}(\mathbf{y})} P_{\boldsymbol{\theta}}(\mathbf{z}'|\mathbf{x})} \nabla \log P_{\boldsymbol{\theta}}(\mathbf{z}|\mathbf{x}),
\end{aligned}$$

Let us switch to Problem (P). By setting $\gamma = 1$, for any $\mathbf{z} \in \mathcal{S}(\mathbf{y})$, we can compute $Q_{\boldsymbol{\phi}^*}$ by

$$Q_{\boldsymbol{\phi}^*}(\mathbf{z}) = \frac{P_{\boldsymbol{\theta}}(\mathbf{z}|\mathbf{x})}{\sum_{\mathbf{z}'\in\mathcal{S}(\mathbf{y})} P_{\boldsymbol{\theta}}(\mathbf{z}'|\mathbf{x})}.$$

and thus $\nabla_{\boldsymbol{\theta}}\ell(\boldsymbol{\theta}, \boldsymbol{\phi}^*)$ can be rewritten as

$$\nabla\ell(\boldsymbol{\theta}) = -\sum_{\mathbf{z}\in\mathcal{S}_{\mathbf{y}}} Q_{\boldsymbol{\phi}^*}(\mathbf{z}) \nabla \log P_{\boldsymbol{\theta}}(\mathbf{z}|\mathbf{x}).$$

For completeness, we also simply prove that the $Q_{\boldsymbol{\phi}^*}$ is the optimal solution of $\min_{\boldsymbol{\phi}} \ell(\boldsymbol{\theta}, \boldsymbol{\phi})$ with $\gamma = 1$. Elaborately, the Lagrangian function of the lower-level problem is

$$\mathcal{L}(\boldsymbol{\phi}; \lambda) = \sum_{\mathbf{z}\in\mathcal{S}_{\mathbf{y}}} Q_{\boldsymbol{\phi}}(\mathbf{z}) \log\left(\frac{Q_{\boldsymbol{\phi}}(\mathbf{z})}{P_{\boldsymbol{\theta}}(\mathbf{z})}\right) - \lambda\Big(\sum_{\mathbf{z}\in\mathcal{S}_{\mathbf{y}}} Q_{\boldsymbol{\phi}}(\mathbf{z}) - 1\Big).$$

By computing its gradient in $Q_{\boldsymbol{\phi}}(\mathbf{z})$, and let it vanish, then

$$\log Q_{\boldsymbol{\phi}^*}(\mathbf{z}) + 1 - \log P_{\boldsymbol{\theta}}(\mathbf{z}) - \lambda = 0$$

should hold for any $\mathbf{z} \in \mathcal{S}_{\mathbf{y}}$. Therefore, we have

$$Q_{\phi^*}(\mathbf{z}) = e^{\lambda-1} P_{\boldsymbol{\theta}}(\mathbf{z}), \quad \sum_{\mathbf{z}\in\mathcal{S}_{\mathbf{y}}} e^{\lambda-1} P_{\boldsymbol{\theta}}(\mathbf{z}) = 1.$$

Putting these two equalities together, we can obtain that

$$Q_{\phi^*}(\mathbf{z}) = \frac{P_{\boldsymbol{\theta}}(\mathbf{z})}{\sum_{\mathbf{z}'\in\mathcal{S}_{\mathbf{y}}} P_{\boldsymbol{\theta}}(\mathbf{z}')},$$

which completes the proof. □

B EXPERIMENTS

B.1 EXPERIMENTAL SETTING

Model architecture. For HWF and Sudoku tasks, we used the LeNet-5 architecture; For SDSP task, we used the multilayer perceptron with 30×30 input neurons, one hidden layers with 128 neurons, and an output layer of 30 neurons.

Batch size and Epoch. For all tasks, the batch size was set to 64. For all comparison methods, and our Stage-I algorithm, the number of epochs is fixed to 1,000. For our Stage-II algorithm, the number of epochs is fixed to 30. We fix $T = 10$ in Alg. 1, i.e., conducting ten random walk steps before one gradient descent step.

Gradient descent algorithm. For all comparison methods, we followed the learning algorithm setting in their respective Github repository. To be specific, RL, MAPO, and SSL conducted the Adam algorithm with learning rate 5e-4. For our approaches, we used the SGD algorithm with learning rate 0.1 in Stage-I, and the Adam algorithm with learning rate 1e-3.

Implementation. For RL, MAPO, and NGS methods, we used the code provided by NGS authors. For SSL methods, we implemented the totally same projection techniques, as well as the random walk strategy, with our approaches.

B.2 FRAMEWORK GUIDELINE

Two key elements in our framework are annealing strategy and projection operator. Hence, we briefly discuss how to set the temperature in annealing strategy and the projection operator.

(1) Intuitively, a good initial temperature should ensure the new state will not be rejected at the first few training epochs. Therefore, setting the initial temperature (e.g., $\gamma_0 = 1$ in our three tasks) to a large value is generally effective. For the hyperparameter setting in the annealing strategy, we recommend to follow that of Nourani & Andresen (1998).

(2) The selection of projection operators in our experiments is a bit arbitrary. Actually, the dimension of the projection space Ω is a trade-off: a larger $\dim(\Omega)$ cannot effectively improve the connectivity of solutions; while a smaller $\dim(\Omega)$ gets more bias introduced the SMT solver. In Feng et al. (2021a), it proposes to evaluate the quality of projection operator via the entropy. A more practical method may be to gradually decrease the dimension of the projection space, and choose the largest $\dim(\Omega)$ without losing too much connectivity.

B.3 ADDITIONAL RESULTS

For the HWF task, we plot the training/test curves of our Stage-I algorithms (Log and Linear) and comparison methods (MAPO, NGS, SSL, and NA) in Figure 4. For our approaches, the random walk step is also counted within the iteration. First, it can be observed that the policy-gradient-based method (MAPO) cannot well fit the training data due to the issue of sparse reward. For the NGS method, it quickly overfits the training set, but cannot improving the symbol accuracy and generalizing to the test set. This result is not surprising because the back-search in NGS is too greedy and hence only works with a good initial model. SSL and NA can be treated as two different variants of our framework, and they learn well during the first few epochs, but then collapse due to the lack of an effective grounding.

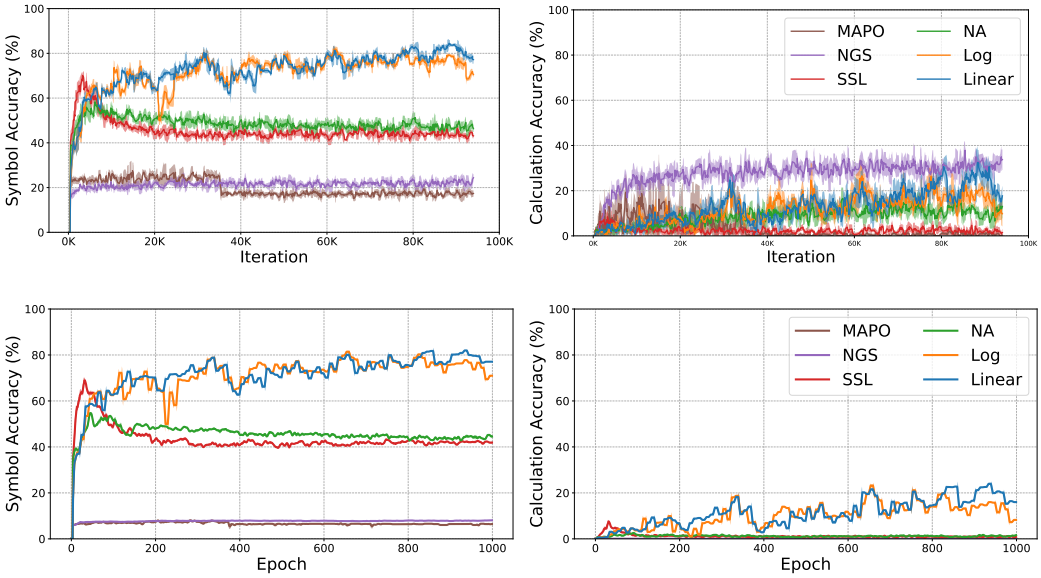

Figure 4: Training curves (the first row) and test curves (the second row) of different approaches. We only plot the curves for some of the methods for brevity. Our approaches (Log and Linear) achieve the best symbol accuracy on the training set, and also generalize better to the test set.

Table 3: Results (%) of additional experiments.

Method	Symbol	Calculation
SSL + Stage-II	17.4	1.41
NA + Stage-II	13.0	0.41
Stage-I + NGS	99.5	96.6

In Table 3, we further report some results of additional experiments on the HWF task. We consider different combinations of our method with the existing methods. We first apply the Stage II algorithm for SSL and NA. However, such variants collapse since they cannot provide a sufficient calculation accuracy, and finally converge to nearly zero calculation accuracy. We next apply the back-search in NGS after our Stage-I algorithm, by initializing with our Stage-I models. This variant can achieve comparable results with that using direct supervision. Note that a bit accuracy drop compared with that in the original NGS paper is due to that we only evaluate the model on length-7 formulas. This result further verifies the effectiveness of our softened symbol grounding. However, the back-search in NGS lacks versatility in more complex settings and is not applicable to other studied tasks.